Pertanika J. Sci. & Technol. 34 (5): 2691 - 2713 (2026)

PERTANIKA JOURNALS

SCIENCE & TECHNOLOGY

Journal homepage: http://www.pertanika.upm.edu.my/

Urban Flooding as a Hydrological Connectivity Problem: An Entropy-Based GIS Assessment in a Low-Relief Tropical City

Fachruddin Abdul Chaidir[1], Masha Nur Salsabiela Menhat[1]*, Mohd Azhafiz Abdullah[1], Muhammad Azraie Abdul Kadir[2], Effi Helmy Ariffin[3], Khairul Nizam Abdul Maulud[4], Ahmad Shakir Mohd Saudi[5], and Hasdinar Umar[6]

[1]Faculty of Maritime Studies, Universiti Malaysia Terengganu, 20130 Kuala Nerus, Terengganu, Malaysia
[2]Neo Environment Technology, Centre for Diploma Studies, Universiti Tun Hussein Onn Malaysia, 84600 Panchor, Johor, Malaysia
[3]Institute of Oceanography and Environment, Universiti Malaysia Terengganu, 20130 Kuala Nerus, Terengganu, Malaysia
[4]Department of Civil Engineering, Faculty of Engineering and Built Environment, Universiti Kebangsaan Malaysia, 43600 UKM Bangi, Selangor, Malaysia
[5]Center for Water Engineering Technology, Malaysia France Institute, Universiti Kuala Lumpur, 43650 Bandar Baru Bangi, Selangor, Malaysia
[6]Department of Ocean Engineering, Faculty of Engineering, Hasanuddin University, 92171 Gowa, South Sulawesi, Indonesia

ABSTRACT

Rapid urban development can intensify drainage limitations and urban flooding in low-lying areas, where hydrological connectivity may be more informative than terrain gradient alone. This study applied an entropy-weighted Geographic Information System (GIS) framework to Taman Sri Muda, Shah Alam, Malaysia, integrating a 0.5 m UAV-derived spatial dataset, seven flood-conditioning factors, and community-informed spatial validation. The factors were elevation, slope, distance to discharge channel, runoff volume, impervious surface ratio, street-drainage intersection density, and Index of Downstream Potentiality Ratio (IDPR). IDPR (0.424) and street-drainage intersection density (0.277) together accounted for 70.1% of the entropy-derived weight. Spatial validation yielded a hit rate of 73.08% (19 of 26 observed flood locations within high- and very-high-hazard zones; 95% binomial confidence interval: 52.4%-88.4%). A targeted sensitivity analysis of the dominant IDPR weight showed only small changes in the combined high- and very-high-hazard areas under perturbations of up

ARTICLE INFO

Article history:
Received: 02 July 2026
Accepted: 02 September 2026
Published: 30 October 2026

DOI: https://doi.org/10.47836/pjst.34.5.07

E-mail addresses:
didirfachrudin24@gmail.com (Fachruddin Abdul Chaidir)
mashanur@umt.edu.my (Masha Nur Salsabiela Menhat)
azhafiz@umt.edu.my (Mohd Azhafiz Abdullah)
mazraie@uthm.edu.my (Muhammad Azraie Abdul Kadir)
effihelmy@umt.edu.my (Effi Helmy Ariffin)
knam@ukm.edu.my (Khairul Nizam Abdul Maulud)
ahmadshakir@unikl.edu.my (Ahmad Shakir Mohd Saudi)
hasdinar.umar@gmail.com (Hasdinar Umar)
* Corresponding author

e-ISSN: 2231-8526

© Universiti Putra Malaysia Press

to ±75%. The framework is therefore presented as a relative, drainage-oriented spatial screening tool for flood-hazard prioritisation in low-relief, data-scarce urban settings, rather than as a predictive model of flood depth or extent.

Keywords: Drainage system performance, entropy-based weighting, GIS-based framework, hydrological connectivity, low-relief urban watershed, UAV-derived mapping, urban flood hazard mapping

INTRODUCTION

Due to the urban heat island effect and rising average rainfall, urban flooding is currently the most common natural disaster and has the potential to affect 379 million people (Manandhar et al., 2023). Urbanisation drives flooding, due to an expansion of impermeable surfaces and development outpacing drainage (Bibi et al., 2023; Du et al., 2019). In low-relief areas, minimal local topographic variation and gentle gradients can reduce drainage efficiency and favour water accumulation. Low-relief landscapes are characterised by limited local relief, so even small elevation differences may strongly influence surface-water pathways (Leopold et al., 1964). This situation is even more pronounced when drainage is obstructed, the floodplain is used inappropriately, and permeability is reduced in small catchment areas (Agonafir et al., 2023; Hassan et al., 2022).

Mapping areas prone to urban flooding is one of the most effective methods for reducing flooding risk across communities by increasing awareness and preparedness for flooding (Fernández & Lutz, 2010). Many methods for flood management have been developed, including remote sensing with machine learning, hydrological process modelling, and participatory methods (Abdessamed & Abderrazak, 2019; Guo & Guan, 2022; Khan et al., 2022). Hydrological and hydraulic models such as HEC-RAS and SWMM offer high physical fidelity but require extensive calibration data and significant computational resources, limiting applicability in data-scarce settings (Abdessamed & Abderrazak, 2019; Feng et al., 2020; Guo & Guan, 2022). Machine learning approaches, including random forest and convolutional neural networks, demonstrate strong predictive performance when large, labelled inventories are available, but are prone to overfitting in small-sample contexts (Guo & Guan, 2022; Khan et al., 2022). Multi-Criteria Decision Analysis (MCDA) integrated with GIS offers a transparent, data-efficient alternative suited for low-data environments, and entropy-based weighting further replaces subjective expert assignment with an objective measure derived from the spatial variability of each conditioning factor (Al-Hinai & Abdalla, 2021; Fernández & Lutz, 2010; Sharma et al., 2024). Most existing methods, however, require large quantities of data, are extremely computationally intensive, and difficult to implement in data-poor regions (Feng et al., 2020; Hassan et al., 2022; Manandhar et al., 2023). There is a clear demand for efficient urban flood-mapping methods that can adapt to the various conditions in which they will be used.

Recent studies in similarly ranked journals have advanced flood susceptibility mapping in several methodological directions. Sharma et al. (2024) applied Shannon entropy, combined with frequency ratio, within a GIS framework to assess flood susceptibility in Chandrapur District, India, demonstrating the utility of entropy-based weighting in data-scarce flat terrain, though without UAV-derived inputs or drainage connectivity factors. Systematic reviews of urban flood susceptibility mapping have identified the entropy weighting method as an objective, data-driven alternative to expert-opinion approaches such as AHP, while also noting that drainage infrastructure parameters remain consistently underrepresented across the literature (Islam et al., 2025). Goumghar et al. (2025) demonstrated the applicability of AHP-MCDM in data-scarce, semi-arid environments (Upper Draa Basin, Morocco; AUC = 0.882), though the study relied on conventional 30 m ASTER DEM inputs rather than high-resolution topographic data. The present work advances on these precedents by: (1) UAV-derived DSM at 0.5 m resolution; (2) explicit operationalisation of hydrological connectivity through IDPR and street-drain intersection density collectively accounting for 70.1% of entropy-derived weight; and (3) multi-source community-informed validation in a Malaysian low-relief tropical urban township.

Hydrological connectivity, the water-mediated transfer within hydrological systems (Dwivedi et al., 2025), encompasses structural and functional dimensions (Bracken et al., 2013). Urbanisation fundamentally alters these dynamics: impervious surfaces reduce infiltration and shorten flow travel times, while engineered infrastructure introduces artificial flow pathways (Du et al., 2015; Singh et al., 2018). In low-relief urban settings, flood susceptibility is governed more by drainage network geometry than terrain gradient (Dell'Aira & Meier, 2025), as terrain-based indices such as the Topographic Wetness Index (TWI) lose discriminatory power in flat areas (Moore et al., 1991). Operationalising hydrological connectivity is therefore essential for characterising flood mechanisms in low-relief tropical cities.

A widely used framework for integrating spatial parameters in flood assessment is Geographic Information Systems (GIS). Although they offer great utility, most GIS methodologies rely on ad hoc, arbitrary weighting, resulting in a high degree of uncertainty. The entropy method is a more sophisticated approach and determines weighting schemes based on the spatial data distribution, improving the consistency, clarity, and replicability of the approach (Al-Hinai & Abdalla, 2021; Liu et al., 2017; Malekinezhad et al., 2021; Sepehri et al., 2019; Sharma et al., 2024).

In addition to methodological improvements, the effectiveness of flood hazard mapping is critically dependent on map validation. Trust and resilience within the community are further enhanced through participation (Abid et al., 2024; Halim et al., 2024), and a comprehensive range of participants increases the utility of the maps for evacuation (Fernández & Lutz, 2010).

Unfortunately, validation methods primarily depend on historical flood inventories. These inventories may be incomplete or updated only intermittently. There is therefore a need for validation approaches that incorporate available on-site evidence, while recognising the limitations of sparse flood inventories for evaluating model performance.

This study addresses an operational gap in drainage-oriented flood-hazard screening for data-scarce, low-relief tropical urban areas. Building on established entropy-MCDA approaches (Malekinezhad et al., 2021; Sepehri et al., 2019), the study contributes: (1) application of a 0.5 m UAV-derived spatial dataset for fine-scale urban analysis; (2) explicit representation of hydrological connectivity through IDPR and street-drainage intersection density, which together account for 70.1% of the entropy-derived weight; (3) multi-source flood-location validation supplemented by community evidence from the December 2021 event; and (4) a targeted sensitivity analysis testing the dominant IDPR weight over ±25%, ±50%, and ±75% perturbations. The objective was not to propose entropy weighting as a new method, but to evaluate a reproducible drainage-oriented screening configuration for prioritising flood-prone locations when calibrated hydraulic model data are unavailable.

METHODOLOGY

Study Area

Taman Sri Muda (Figure 1) is a highly populated, low-relief, flood-prone area along the Klang River (Section 25, Shah Alam, Selangor, Malaysia; 3.0471° N, 101.5275° E). It has



Figure 1. Area of study

a population of 38,812 people in an area where the average population density for Shah Alam is 3,068 people/km². This flood-prone area has poor natural drainage, excessive impervious surfaces, and significant elevation reduction (Dewan Negeri Selangor, 2022; Muhamad Azizi & Teriman, 2023). The location and infrastructure of Taman Sri Muda make it an ideal setting for studying drainage-based flood-reduction methods in densely populated, low-relief urban areas. December 2021 was the most extreme flooding event to date and was caused by 280 mm of rainfall (Nooryati, 2022).

Flood Conditioning Factors: Selection Criteria and Data Preparation

Numerous interconnected physical and anthropogenic factors create complex, nonlinear direct drivers of flood hazard. The initial step was determining the conditioning factors. Since environmental and hydrological conditions vary greatly across geographic locations, determining conditioning factors is essential. In accordance with past studies, flood conditioning factors can be described in the following three ways. First, discrete criteria, which are primarily static physical characteristics of the landscape, for example, slope and elevation; second, integrated criteria, which are processes of hydrology that are sustained and intensified, for example, the volume of runoff; and third, the criteria of connectivity, which describe the spatial connection and interaction of flow between the elements of drainage combined. These three categories of conditioning factors are summarised in Table 1.

Table 1
Factors Influencing Flood Hazard Mapping

Category	Criterion	Resolution	Source	Former Studies
Topography	Elevation	0.5 m x 0.5 m	UAV (2023)	Fernández & Lutz, 2010; Malekinezhad et al., 2021; Tang et al., 2018
	Slope	0.5 m x 0.5 m	UAV (2023)	Fernández & Lutz, 2010; Malekinezhad et al., 2021; Tang et al., 2018
Hydrology	Distance to discharge channel	0.5 m x 0.5 m	UAV drainage (2023)	Fernández & Lutz, 2010; Malekinezhad et al., 2021
	IDPR	0.5 m x 0.5 m	UAV elevation/ drainage (2023)	Fernández & Lutz, 2010; Malekinezhad et al., 2021
	Runoff Volume	0.5 m x 0.5 m	UAV land cover FAO soil 2021 rainfall	Malekinezhad et al., 2021
	ISR	0.5 m x 0.5 m	UAV orthomosaic (2023)	Du et al., 2015; Feng et al., 2020
Human activity	Street-drainage intersection	0.5 m x 0.5 m	UAV drainage + OSM roads	Malekinezhad et al., 2021

The proposed analytical framework combines the findings of research by Sepehri et al. (2019), Malekinezhad et al. (2021), and Fernández and Lutz (2010) using a structured Multi-Criteria Decision Analysis (MCDA) framework to integrate evidence from raster and vector datasets and the field (Figure 2). The following seven primary factors constitute the flood-hazard assessment: elevation, slope, distance to discharge channel, runoff volume, street-drainage network intersection density, Index of Downstream Potentiality Ratio (IDPR), and Impervious Surface Ratio (ISR). The UAV-derived dataset at 0.5 m resolution provides a breakdown of fine-scale hydrological connectivity and topographical variance. The resulting flood-hazard index is a relative spatial screening index and should not be interpreted as a direct estimate of flood depth or flood extent.

Elevation

The study used an existing UAV-derived elevation dataset from the 2023 project survey, resampled to a 0.5 m raster for the present GIS analysis. Because the UAV acquisition and primary photogrammetric processing were undertaken as part of the source project rather than specifically for this study, only processing steps documented in the project materials are reported here. The project workflow used Agisoft Metashape for image alignment, pixel-based dense stereo reconstruction, mesh and point-cloud generation, and export of orthomosaic and Digital Surface Model (DSM) products in TIFF format. The elevation products were referenced to the project coordinate framework in UTM Zone 47N and related to the JUPEM mean sea level datum. Detailed flight metadata, formal ground-control-point documentation, and an independent vertical RMSE assessment were not available to the present study; this limitation was therefore acknowledged rather than inferred. The UAV-derived elevation surface was used for elevation classification and as the terrain input for

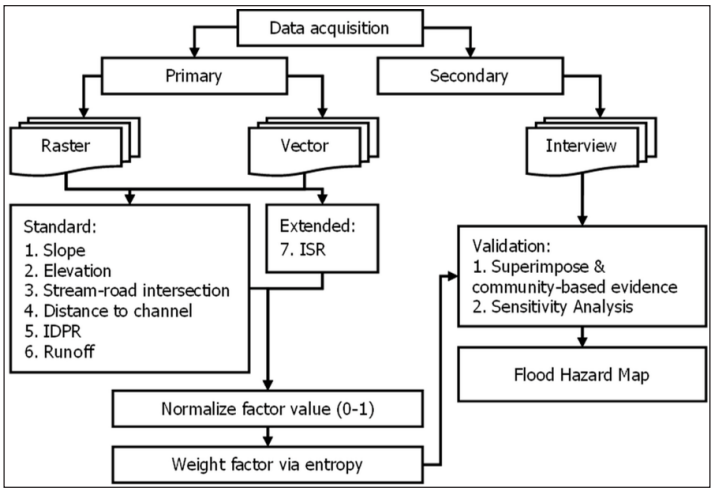

Figure 2. Methodology framework

slope and surface-flow analyses in ArcGIS Pro 3.4. The elevation surface was segmented into classes based on its value distribution and surface characteristics (Figure 3a). Low-elevation areas were assigned higher flood-hazard relevance because they represent preferential zones for surface-water accumulation (Malekinezhad et al., 2021).

Slope

Slope was derived in degrees from the UAV-derived elevation surface using ArcGIS Pro 3.4 (Figure 3b). Slope affects flow direction and velocity and is a well-documented flood-conditioning factor (Fernández & Lutz, 2010). In low-relief terrain, lower slopes reduce surface-flow velocity and favour water accumulation and waterlogging; accordingly, lower slope values were interpreted as representing greater flood-hazard potential (Malekinezhad et al., 2021; Tang et al., 2018).

Street-Drainage Network Intersection Density

The drainage-channel network was derived from the UAV-based terrain surface using flow-direction and flow-accumulation analyses in ArcGIS Pro 3.4, whereas the road network was obtained from OpenStreetMap (OSM) as road centreline data. Network-intersection points were identified by spatially overlaying the derived drainage network and the OSM road network. Kernel Density Estimation was then applied to the intersection points using a 100 m search radius and a 0.5 m output cell size, consistent with the analysis raster resolution. The resulting density surface represents the spatial concentration of street-drainage intersections per unit area and was normalised to a 0-1 scale before entropy weighting (Figure 3c). Roads can rapidly convey surface runoff toward drainage channels, while drainage-road intersections may act as local convergence nodes during intense rainfall; therefore, higher intersection density was interpreted as greater flood-hazard potential (Pimenta et al., 2025; Singh et al., 2018).

Runoff

Runoff volume was estimated using the Soil Conservation Service-Curve Number (SCS-CN) method, widely applied in urban flood studies for its ability to link rainfall with catchment retention characteristics (Malekinezhad et al., 2021). The method quantifies runoff as:

$$Q = \frac{(P-0.2S)^2}{(P+0.8S)}, for P \geq 0.2S \quad [1]$$

$$S = \frac{25400}{CN} - 254 \quad [2]$$

Equation 1 was used to calculate runoff depth (Q), while Equation 2 was applied to determine the potential maximum retention (S) based on the Curve Number (CN). Here, Q represents runoff depth (mm), P represents rainfall (mm), S represents potential maximum retention (mm), and CN represents land-surface infiltration characteristics. The Gleysol classification used by the source project was taken from FAO global soil-mapping resources accessed through the FAO Soils Portal. Rainfall represented the December 2021 extreme event (approximately 280 mm). Antecedent Moisture Condition (AMC) II was assumed to represent average antecedent soil moisture. CN values were assigned from UAV orthomosaic-based land-cover classes: fully connected impervious surfaces (roads and rooftops), CN = 98; partially connected impervious surfaces, CN = 90; and vegetated or open areas, CN = 61, following the adopted event-based SCS-CN setup and the approach of Malekinezhad et al. (2021). The runoff layer, therefore, represented a static, event-based index rather than a calibrated multi-event runoff model, and its applicability beyond the 280 mm event should be interpreted with caution.

Index of Downstream Potentiality Ratio (IDPR)

IDPR was implemented from the UAV-derived elevation surface through a surface-flow workflow in ArcGIS Pro 3.4. The raw IDPR was expressed as the ratio of the flow length from a cell to its downstream sink relative to the maximum flow length in the study area. Subsurface drainage pipes were not included in this surface-routing representation. Because the study area is low-relief, the D8 representation and the omission of below-ground drainage may introduce uncertainty in local flow paths; these limitations were explicitly considered in interpreting the resulting hazard index.

$$IDPR_i = \frac{L_i}{L_{max}} \quad [3]$$

Equation 3 was used to calculate the IDPR for each pixel using the downstream flow length and its maximum value within the study area. Where IDPR is the hydrological-connectivity index of a pixel (dimensionless), L is the flow length from the pixel to the nearest theoretical downstream sink, and Lmax is the maximum flow length used for normalisation (Malekinezhad et al., 2021). A smaller raw IDPR corresponds to a shorter downstream flow path and was interpreted as greater flood-hazard potential. For hazard standardisation, IDPR was therefore treated as an inverse (cost-type) criterion, so that smaller raw values receive higher normalised hazard scores. This treatment preserves the intended physical interpretation of short downstream flow paths in the weighted overlay. IDPR was preferred to the Topographic Wetness Index (TWI) because flow-path length can retain spatial discrimination in low-relief terrain where slope-dependent indices may become unstable as local slope approaches zero (Lane et al., 2009; Moore et al., 1991).

Impervious Surface Ratio (ISR)

The Impervious Surface Ratio (ISR) is a metric used to gauge how changes in land surfaces caused by human activities affect local hydrological systems. In cities, surging runoff and flood risks are a direct result of rapid land development via building construction, road and pavement installation, and other similar activities (Dell'Aira & Meier, 2025; Du et al., 2015; Ogden et al., 2011). ISR data for each land unit came from UAV land-cover classifications (Figure 3f). ISR data were used to indicate potential runoff, with higher ISR values indicating a greater probability of runoff.

Distance to Discharge Channel

Distance to discharge channels indicates proximity to the surface drainage network (Figure 3g). Euclidean Distance was calculated in ArcGIS Pro 3.4, with shorter distances interpreted as greater flood-hazard potential because locations close to drainage pathways may be more directly exposed to local surcharge, overflow, or convergent surface flow during intense rainfall. For weighted integration, the distance layer was inversely standardised so that smaller raw distances receive larger normalised hazard scores. Euclidean distance was selected as a transparent and computationally efficient approximation of drainage accessibility in the densely built study area. The method does not account for barriers such as buildings and elevated road embankments, or for the hydraulic capacity of drains; these simplifications are acknowledged as limitations (Fernández & Lutz, 2010; Malekinezhad et al., 2021).

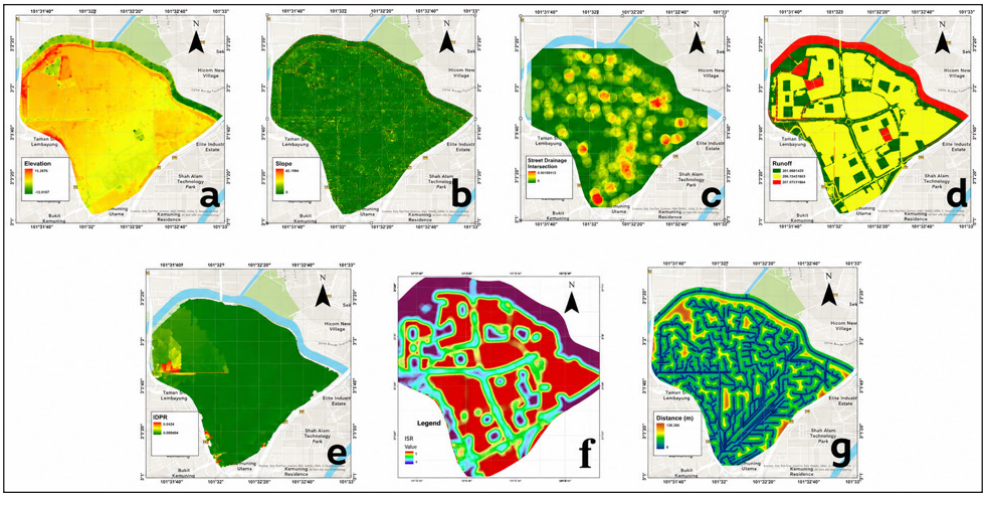

Figure 3. Flood conditioning factors used in this study: (a) Elevation, (b) Slope, (c) Street drainage network intersection density, (d) Runoff, (e) IDPR, (f) ISR, (g) Distance to discharge channel

Processing: Determination of Weights for Flood Conditioning Factors and Mapping

The entropy method reduces reliance on subjective MCDA weighting by quantifying the information contribution of each factor from its spatial variability (Malekinezhad et al., 2021; Sharma et al., 2024). Before entropy calculation, factor values were normalised to a common 0-1 hazard scale. Runoff volume, ISR, and street-drainage intersection density were treated as benefit-type criteria, for which larger raw values represent greater hazard. Elevation, slope, IDPR, and distance to discharge channel were treated as cost-type criteria and inversely standardised so that smaller raw values represent greater hazard. This directionality ensured that all normalised layers have a consistent interpretation: larger normalised values indicate greater flood-hazard potential.

$$P(x) = \frac{\mathrm{x} - \min(x)}{\max(x) - \min(x)} \quad [4]$$

$$P(x) = \frac{\max(\mathrm{x}) - \mathrm{x}}{\max(x) - \min(x)} \quad [5]$$

Equation 4 was used to normalise benefit-type criteria, while Equation 5 was applied to inversely normalise cost-type criteria, ensuring a consistent flood-hazard scale across all conditioning factors.

The equation for measuring the entropy for factor j is expressed as follows:

$$H_j = -k \sum_{i=1}^{n} p_{ij} \ln(p_{ij}) \quad [6]$$

Equation 6 was used to calculate the entropy value for each flood-conditioning factor based on the distribution of its normalised values across the study area.

where p_{ij} defines the quantity for the factor j at the spatial unit i., n is the number of spatial units, and $k = 1/(\ln n)$ is the normalisation constant. Smaller entropy values result in greater spatial variability and a greater contribution to information. The determination of the entropy-based weight for each factor was as follows:

$$w_j = \frac{1 - H_j}{\sum_{j=1}^{m} (1 - H_j)} \quad [7]$$

Equation 7 was applied to determine the entropy-based weight of each flood-conditioning factor, reflecting its relative contribution to the overall flood-hazard assessment. Here, m represents the total number of flood-conditioning factors.

Normalisation was performed across all raster cells within the complete study area boundary rather than only at validation points, so the entropy weights reflect the full spatial distribution of each factor. Zero values in the normalised raster were replaced with a small constant (p = 0.0001) before entropy calculation to avoid undefined logarithmic terms. All seven factors were directionally standardised to a common hazard orientation prior to entropy weighting: higher normalised values consistently indicate higher hazard. Runoff volume, ISR, and street-drainage intersection density were standardised as benefit-type criteria, whereas elevation, slope, IDPR, and distance to channel were inversely standardised as cost-type criteria. The continuous FHI was classified into five hazard classes (very low, low, moderate, high, and very high) using Jenks Natural Breaks.

$$\mathrm{FHI} = \sum_{j=1}^{m} w_j \cdot P_j \qquad [8]$$

Equation 8 was used to calculate the final Flood Hazard Index (FHI) by integrating the normalised flood-conditioning factors with their corresponding entropy-derived weights, where P_j represents the normalised raster layer of factor j, and w_j represents its entropy-derived weight. The continuous FHI values were then divided into five hazard classes (very low, low, moderate, high, and very high) using the Natural Breaks (Jenks) classification, which maximises differences between classes and minimises variance within a class.

Validation and Robustness Assessment of Flood Hazard Mapping

The flood hazard map was evaluated using spatial overlay validation, community-based confirmation, and a targeted robustness analysis given the limited official flood inventory. The 26 observed flood-occurrence locations were compiled from on-site documentation, official post-flood reports, media records, and interviews with residents who directly experienced the December 2021 event; source-specific counts were not retained separately and were therefore not reconstructed retrospectively. The model agreement was summarised as the proportion of observed flood locations falling within the high and very high hazard classes. Robustness was evaluated as a one-factor-at-a-time sensitivity test of the dominant IDPR weight only, using perturbations of ±25%, ±50%, and ±75% relative to its baseline value. The analysis, therefore, tests sensitivity to uncertainty in the highest-weighted factor and should not be interpreted as a full multivariate uncertainty analysis.

RESULTS AND DISCUSSIONS

Results of Weight Determination for Flood Conditioning Factors

Entropy-based weighting estimates each factor's relative contribution from spatial variability. Factors with lower entropy values exhibit greater spatial heterogeneity and

contribute more information for flood hazard differentiation (Al-Hinai & Abdalla, 2021; Haghizadeh et al., 2017; Malekinezhad et al., 2021).

IDPR showed the lowest entropy (0.935) and the largest entropy-derived weight (0.424), indicating the greatest contribution to spatial information among the seven factors. Street-drainage intersection density ranked second (entropy = 0.958; weight = 0.277). Runoff volume (entropy = 0.979; weight = 0.140) and ISR (entropy = 0.981; weight = 0.124) had intermediate contributions. Distance to drainage, slope, and elevation each had entropy values of 0.998, with corresponding weights of 0.015, 0.010, and 0.010, respectively. The near-uniform elevation and slope surfaces therefore contributed comparatively little spatial discrimination in this low-relief setting (Table 2).

In Taman Sri Muda, the low-relief terrain limits the spatial contrast provided by elevation and slope, whereas the organisation of drainage pathways and their interaction with the built environment provide stronger spatial differentiation. The large weights assigned to IDPR and street-drainage intersection density were therefore interpreted as evidence that drainage connectivity is a dominant discriminator within this relative hazard model. Runoff volume and ISR remain important secondary factors, representing runoff generation and imperviousness, but their effects were interpreted together with the capacity and organisation of the drainage system (Ogden et al., 2011).

The model interpretation is consistent with post-flood accounts that described drainage-system overload during the December 2021 event. This agreement does not establish hydraulic causality because drain capacity, pipe geometry, pumping, and sluice operations were not explicitly simulated. Rather, the entropy-weighted spatial pattern indicates that connectivity-related factors provide stronger discrimination than topographic variation within the study area. The result supports the use of the framework for first-order drainage-oriented screening and prioritisation, while calibrated hydraulic modelling remains necessary for quantitative assessment of flood depth, conveyance capacity, and infrastructure performance (Liu et al., 2017; Singh, 1997).

Table 2
Results of Entropy-based weighting showing the relative contribution of flood-conditioning factors to urban flood hazard mapping

Rank	Flood-conditioning factor	Entropy (Hj)	Divergence (dj)	Weight (wj)
1	IDPR	0.935	0.065	0.424
2	Street drainage intersection density	0.958	0.042	0.277
3	Runoff volume	0.979	0.021	0.140
4	Impervious surface ratio (ISR)	0.981	0.019	0.124
5	Distance to drainage	0.998	0.002	0.015
6	Slope	0.998	0.002	0.010
7	Elevation	0.998	0.002	0.010

Flood Hazard Map Based on Entropy Weighting

Flood hazard mapping is shown in Figure 4. The map was constructed from the entropy-derived weights through weighted overlay in ArcGIS Pro 3.4 and classified into five Natural Breaks (Jenks) classes. The resulting pattern shows localised concentrations of high and very high relative hazard associated with the drainage framework and the dominant connectivity factors.

The hazard map (Figure 4) exhibits an uneven spatial distribution. High and very high zones are concentrated mainly within densely built residential areas, particularly in the central and eastern portions of the study area, where impervious surfaces and drainage-road interactions are prominent. Based on the GIS areal output, very low, low, moderate, high, and very high classes occupy 0.483, 0.424, 1.067, 1.087, and 0.338 km², respectively. These correspond to approximately 14.22%, 12.46%, 31.40%, 31.99%, and 9.94% of the study area. Thus, moderate-to-very-high classes account for 73.32%, whereas low and very low classes together account for 26.68%. These classes represent relative spatial screening priorities rather than deterministic inundation depth or extent.

These results match previously documented findings. IDPR and intersection density received the highest-ranking weights, and the analysis concludes that the pattern of flood hazards is influenced primarily by the drainage system's connectivity and performance. In most flat, built-up, urban areas, drainage and road networks concentrate flows. Blockage of drainage and road networks leads to rapid water accumulation at intersections (Zhou et al., 2022). These results are consistent with other studies (DeSousa et al., 2024; Liu & Zhang, 2025), which show that the characteristics of urban drainage systems and the

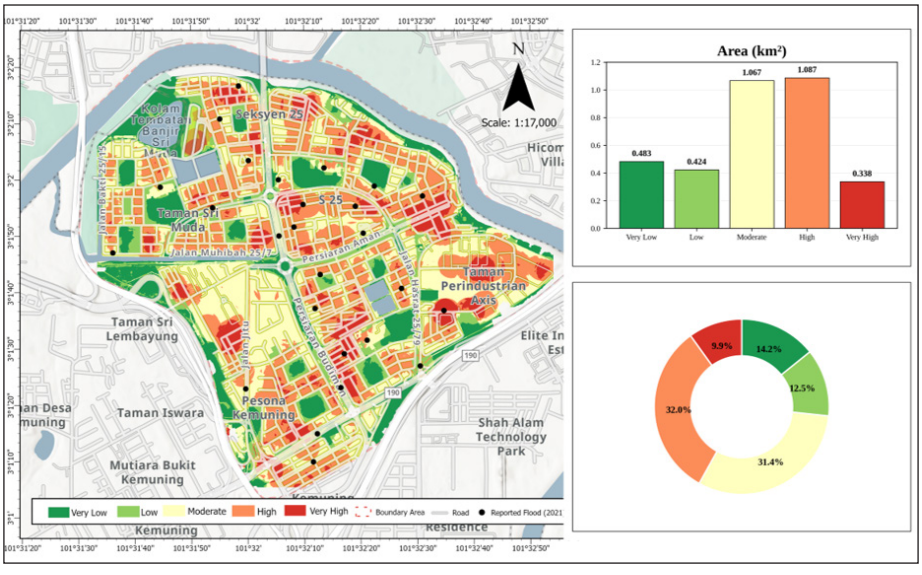

Figure 4. Spatial distribution and areal proportion of urban flood hazard classes in Taman Sri Muda

degree of connectivity dominate the location and the intensity of flooding, more so than the topography of the area. The moderate zones are areas that experience substantial runoff but have drainage systems only partially overloaded. The intermediate weights assigned to runoff and ISR indicate that runoff formation depends on the drainage system's capacity to receive flow (Ahmad et al., 2024; Hassan et al., 2022).

Low- to very-low-hazard zones are characterised by an increasing proportion of green open space, resulting in enhanced permeability and decreased flow velocities (Bai et al., 2018; De Vleeschauwer et al., 2014; Liu & Zhang, 2025). However, green zones adjacent to rivers or floodplains are susceptible to backwater and overflow (Yusuf et al., 2023). The 2021 flood fully inundated almost the entire Taman Sri Muda, including the green zones. This shows that the hazard map expresses the level of risk in relative terms, not that the zones are risk-free.

While some flood-susceptibility studies emphasise topographic controls (Gebremichael et al., 2025; Nizar et al., 2024), the present results suggest that topography provides less spatial discrimination in this flat, highly urbanised setting, where built surfaces and drainage connectivity exert stronger local contrasts (Komori et al., 2022). Post-flood documentation also describes drainage-system overload during the 2021 event. The spatial correspondence between the relative hazard pattern and available flood-positive locations supports prioritising drainage assessment, connectivity bottlenecks, and obstruction management in high and very high zones. Measures addressing imperviousness and urban green space should be considered complementary rather than interpreted as substitutes for hydraulic-capacity assessment.

Results of Spatial Validation and Robustness Analysis

Flood points were integrated into the model to evaluate spatial agreement between observed flood impacts and the mapped hazard pattern in a context where a complete formal flood inventory was unavailable. The 26 geocoded flood-occurrence locations were compiled from four source types: on-site documentation, official post-flood reports (Dewan Negeri Selangor, 2022; Nooryati, 2022), media records, and community interviews. Source-specific counts were not retained separately. Community interviews involved five (n = 5) flood-affected residents of Taman Sri Muda who directly experienced the December 2021 event. Verbal consent was obtained before face-to-face interviews covering flood experience, water depth and duration, rescue response, drainage conditions, and post-flood recovery. Interview-derived locations were referenced to respondents' residential/locality information within the study area rather than interpreted as instrument-surveyed flood coordinates. Respondents' identities were not reported, and personally identifiable information was not retained in the analysis. Interview evidence was used as contextual corroboration and triangulated with documentary sources rather than treated as a statistically representative

sampling. Potential recall bias, uncertainty from locality-based geocoding, media selection bias, and the absence of probabilistic sampling were therefore recognised.

The use of community-reported and digitally mediated flood-location data also requires explicit attention to privacy and data governance. In this study, interview-derived information was used only for spatial validation; identities were not reported, and personally identifiable information was not retained. This conservative approach is consistent with broader privacy-preserving principles in connected data environments, including secure auditing of cloud-based IoT data and decentralised/federated approaches that reduce unnecessary centralisation of user information (Khan et al., 2024; Ullah et al., 2025). These studies are cited to frame data-governance practice rather than to claim that their technical architectures were implemented in the present flood study.

As shown in Table 3, 73.08% of the observed flood-occurrence locations (19 of 26) fell within the high and very high hazard classes, with a 95% binomial confidence interval of 52.4%-88.4%. A further 26.92% (7 of 26) fell within the moderate class, and none of the available flood points fell within the low or very low classes. This result is reported as a spatial hit rate (success ratio), not as a spatial correlation coefficient. Because the inventory contains only flood-positive locations and no systematically verified non-flood controls, the result supports spatial concordance with observed flood locations but cannot assess specificity or false-positive performance.

The December 2021 flood is the most extensively documented event used in this study. Community accounts indicated recurrent local flooding and described the 2021 event as particularly severe, with rapid water-level rise and prolonged inundation. These observations provide contextual support for interpreting the mapped hazard pattern but do not constitute independent calibration data. More complete predictive validation would require a structured inventory containing both flood-affected and verified non-flood locations, allowing measures such as AUC-ROC, sensitivity, specificity, precision-recall, and false-positive rates. Such non-flood reference data were not available for the same

Table 3
Distribution of observed flood-occurrence points across flood-hazard classes used for spatial validation

Flood hazard class	Number of points (n)	Percentage (%)
Very low	0	0.00
Low	0	0.00
Moderate	7	26.92
High	13	50.00
Very high	6	23.08
High + Very high	19	73.08
Total	26	100.00

Note. Source Adapted from: (flood case 2021)

event; consequently, these metrics were not calculated, and the 73.08% value was retained only as a flood-point hit rate.

Robustness Analysis

A targeted robustness analysis tested the sensitivity of the mapped hazard pattern to the dominant IDPR weight. The baseline IDPR weight was perturbed by ±25%, ±50%, and ±75% on a per-factor basis, while the remaining factor structure was retained for comparison. Results are summarised in Table 4.

Across the tested scenarios, the area classified as high- or very-high hazard changed only modestly (approximately 1%-3%) even under a ±75% perturbation of the IDPR weight. Some weight-reduction scenarios produced slight increases rather than monotonic decreases in hazard area because the relative contribution of the remaining factors, particularly street-drainage intersection density and runoff, becomes more influential in the weighted overlay. These results indicate that the mapped high-hazard pattern is only weakly sensitive to large changes in the dominant IDPR weight. However, the analysis was restricted to one-factor-at-a-time perturbation of IDPR and does not demonstrate robustness to simultaneous uncertainty in all seven factors. Leave-one-factor-out analysis, simultaneous weight perturbation, and Monte Carlo propagation of terrain uncertainty were not conducted. The result should therefore be interpreted as a targeted sensitivity check supporting the stability of first-order screening priorities, not as comprehensive uncertainty quantification.

Improvement in Drainage-Based Urban Flood Management Framework

In low-relief urban areas, drainage capacity and connectivity can strongly influence where flooding concentrates in response to rainfall forcing. In this case study, the dominance of IDPR (weight 0.424), street-drainage intersection density (0.277), and the spatial

Table 4
Results of the robustness analysis showing changes in the areas of high and very high flood hazard zones under systematic perturbations to the IDPR weight.

Scenario	Description	High & Very High Areas (km²)	Change from Original (%)
Original	Entropy-derived weights	1.425	–
Scenario +25%	IDPR weight increased 25%	1.448	2%
Scenario -25%	IDPR weight decreased 25%	1.439	1%
Scenario +50%	IDPR weight increased 50%	1.455	2%
Scenario -50%	IDPR weight decreased 50%	1.464	3%
Scenario +75%	IDPR weight increased 75%	1.479	3%
Scenario -75%	IDPR weight decreased 75%	1.472	3%

correspondence between modelled hazard and the 2021 flood impact in Taman Sri Muda indicate that drainage-related factors are major spatial controls on flood concentration. The results are consistent with the findings of Agonafir et al. (2023) and Bibi et al. (2023) in that inadequate drainage systems are the primary factor in flood hazards in rapidly urbanising areas.

Flood risk management, especially in the urban context, requires integrated solutions. Stand-alone interventions, such as channel enlargement, are inadequate in the long term but can be more effective when used in conjunction with restorative nature-based interventions (Zhou, 2014). In Malaysia, flood risk management is the result of many different agencies operating at different administrative levels, often leading to funding limitations that leave drainage systems incomplete, with the most critical system bottlenecks unresolved (Rosmadi et al., 2023).

High and very high hazard zones represent the first prioritisation level for drainage inspection, capacity assessment, identification of hydraulic bottlenecks, and obstruction management, whereas moderate zones warrant preventive maintenance and runoff management. An adaptive flood-management framework can combine spatial diagnosis, periodic monitoring, cross-sectoral collaboration, and stepwise implementation. Citizen observatories and digital reporting systems can improve local flood information when public feedback is integrated into formal planning processes (Wehn et al., 2015).

Although developed for precision-agriculture applications rather than flood modelling, context-aware IoT studies demonstrate a transferable principle: distributed local sensing can support data-driven environmental decision-making. IoT-assisted soil-fertility mapping links real-time field conditions to context-specific recommendations (Khan et al., 2022), while data-driven evapotranspiration studies show how limited environmental observations can support water-management decisions (Bashir et al., 2023; Khan et al., 2022). These studies are cited only as methodological analogues for future adaptive monitoring and are not used as evidence for the validity of the present flood-hazard model.

The framework illustrated in Figure 5 presents an adaptive, multi-level, drainage-based urban flood-management pathway that links local diagnosis and mitigation with longer-term, coordinated government action. At the local level, GIS-based flood vulnerability mapping and the drainage-connectivity indicators identified in this study provide the basis for diagnosing likely drainage failure mechanisms and defining management priorities, including drainage-oriented mitigation, flood-hotspot zoning, emergency-access planning, and rescue assembly points.

The framework then links ad hoc drainage mitigation and community self-mitigation measures to monitoring of flood recurrence and drainage performance. If local conditions remain unstable, the process escalates to cross-agency discussion, budgeted drainage upgrading, and coordinated implementation, followed by renewed monitoring. Figure 5

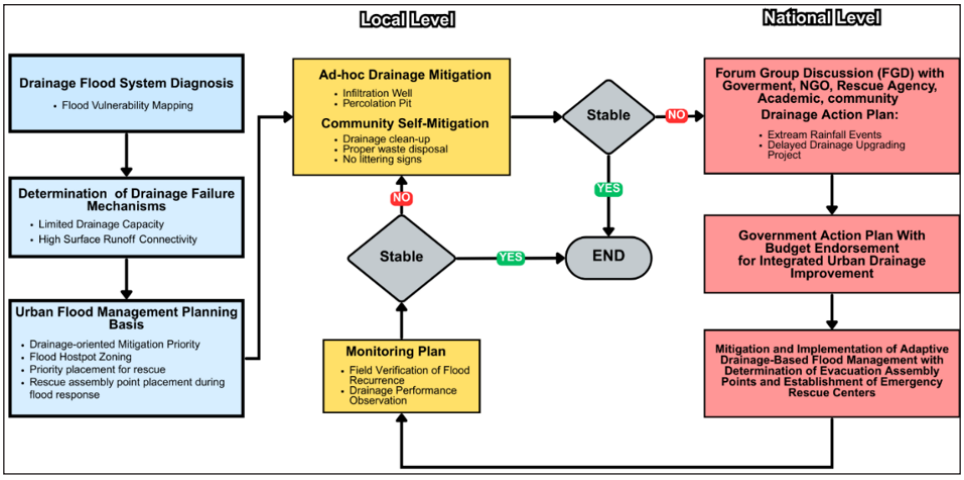

Figure 5. Framework for adaptive drainage-based urban flood management

is therefore intended as an adaptive management pathway informed by the study's spatial screening outputs, rather than as a calibrated hydraulic or engineering design model.

LIMITATIONS

Several limitations should be considered when interpreting the results. First, the flood hazard map is a relative spatial screening index and should not be interpreted as a predictive model of flood depth or extent. Second, the validation event occurred in December 2021, whereas the UAV dataset was acquired in 2023. Infrastructure and land-cover changes between these dates could not be independently verified; this temporal mismatch, therefore, introduces uncertainty that cannot be quantified from the available records. Third, the SCS-CN runoff factor was derived from a single approximately 280 mm rainfall event and was not calibrated across multiple storms. Fourth, rainfall was treated as spatially uniform, so local sub-catchment rainfall variability was not represented. Fifth, subsurface drainage pipes, pipe dimensions, invert levels, pumping, and sluice-gate operations were not explicitly modelled in the surface-routing analysis. Sixth, Kernel Density-based street-drainage intersection density and Euclidean distance to channel are simplified spatial proxies rather than hydraulic-capacity measures. Seventh, potential conceptual overlap exists among ISR, runoff volume, and street-drainage intersection density because all partially reflect urban imperviousness and drainage organisation. Eighth, the community component is based on five residents and is vulnerable to recall, locality-geocoding, and selection biases; the 26-point flood inventory also lacks verified non-flood controls. Ninth, the robustness analysis perturbed only the IDPR weight and therefore does not constitute a comprehensive multivariate uncertainty analysis. Finally, detailed UAV flight metadata, formal GCP documentation, and an independent vertical RMSE were unavailable to this

study. These limitations reinforce the interpretation of the FHI as a first-order, drainage-oriented prioritisation tool rather than a substitute for calibrated hydraulic simulation.

CONCLUSION

This study shows that within the low-relief, densely urbanised setting of Taman Sri Muda, spatial differentiation of relative flood hazard is dominated by drainage connectivity indicators rather than by topographic variation alone. IDPR and street-drainage intersection density received the two largest entropy-derived weights (0.424 and 0.277, respectively), together accounting for 70.1% of the total weight. The spatial hit rate of 73.08% (19/26; 95% binomial CI: 52.4%-88.4%) indicates agreement between the high/very high hazard classes and the available flood-positive locations, while the targeted IDPR sensitivity analysis indicates that the mapped high-hazard area changes only modestly under substantial perturbation of the dominant weight. These findings support the use of the framework as a relative drainage-oriented screening approach, not as a deterministic flood-depth model.

The principal contribution of the study is the operational integration of fine-resolution UAV-derived spatial data, entropy weighting, and explicit drainage-connectivity factors in a data-scarce low-relief urban setting. This combination reduces dependence on subjective expert weighting and provides a transparent basis for prioritising locations for further drainage inspection. The framework should nevertheless be applied with caution because the validation inventory is flood-positive only, the UAV and validation dates are temporally mismatched, subsurface hydraulic infrastructure is not represented, and the available sensitivity analysis addresses only the dominant IDPR weight.

This study highlights a critical research gap in coupling connectivity-based GIS frameworks with dynamic hydrological-hydraulic modelling to capture the temporal evolution of urban flooding. The absence of standardised and continuously updated urban flood inventories further constrains robust validation and model transferability. Addressing these gaps through integrated modelling and systematic data collection is essential for advancing evidence-based, drainage-oriented urban flood risk management.

ACKNOWLEDGEMENTS

This research was supported by the Ministry of Higher Education (MOHE) through the Fundamental Research Grant Scheme (FRGS), Grant No. FRGS/1/2023/TK02/UMT/02/1. The authors would like to thank the MOHE for the financial support. We also thank our colleagues and institutions for their contributions to this research.

REFERENCES

Abdessamed, D., & Abderrazak, B. (2019). Coupling HEC-RAS and HEC-HMS in rainfall–runoff modeling and evaluating floodplain inundation maps in arid environments: Case study of Ain Sefra city, Ksour

Mountain. SW of Algeria. *Environmental Earth Sciences, 78*(19), Article 586. https://doi.org/10.1007/s12665-019-8604-6

Abid, S. K., Sulaiman, N., Al-Wathinani, A. M., & Goniewicz, K. (2024). Community-based flood mitigation in Malaysia: Enhancing public participation and policy effectiveness for sustainable resilience. *Journal of Global Health, 14*, Article 04290. https://doi.org/10.7189/jogh.14.04290

Agonafir, C., Lakhankar, T., Khanbilvardi, R., Krakauer, N., Radell, D., & Devineni, N. (2023). A review of recent advances in urban flood research. *Water Security, 19*, Article 100141. https://doi.org/10.1016/j.wasec.2023.100141

Ahmad, S., Jia, H., Ashraf, A., Yin, D., Chen, Z., Ahmed, R., & Israr, M. (2024). A novel GIS-SWMM-ABM approach for flood risk assessment in data-scarce urban drainage systems. *Water, 16*(11), Article 1464. https://doi.org/10.3390/w16111464

Al-Hinai, H., & Abdalla, R. (2021). Mapping coastal flood susceptible areas using Shannon's entropy model: The case of Muscat governorate, Oman. *ISPRS International Journal of Geo-Information, 10*(4), Article 252. https://doi.org/10.3390/ijgi10040252

Bai, T., Mayer, A. L., Shuster, W. D., & Tian, G. (2018). The hydrologic role of urban green space in mitigating flooding (Luohe, China). *Sustainability, 10*(10), Article 3584. https://doi.org/10.3390/su10103584

Bashir, R. N., Khan, F. A., Khan, A. A., Tausif, M., Abbas, M. Z., Shahid, M. M. A., & Khan, N. (2023). Intelligent optimization of reference evapotranspiration (ETo) for precision irrigation. *Journal of Computational Science, 69*, Article 102025. https://doi.org/10.1016/j.jocs.2023.102025

Bibi, T. S., Reddythta, D., & Kebebew, A. S. (2023). Assessment of the drainage systems performance in response to future scenarios and flood mitigation measures using stormwater management model. *City and Environment Interactions, 19*, Article 100111. https://doi.org/10.1016/j.cacint.2023.100111

Bracken, L. J., Wainwright, J., Ali, G. A., Tetzlaff, D., Smith, M. W., Reaney, S. M., & Roy, A. G. (2013). Concepts of hydrological connectivity: Research approaches, pathways and future agendas. *Earth-Science Reviews, 119*, 17-34. https://doi.org/10.1016/j.earscirev.2013.02.001

De Vleeschauwer, K., Weustenraad, J., Nolf, C., Wolfs, V., De Meulder, B., Shannon, K., & Willems, P. (2014). Green–blue water in the city: Quantification of impact of source control versus end-of-pipe solutions on sewer and river floods. *Water Science and Technology, 70*(11), 1825-1837. https://doi.org/10.2166/wst.2014.306

Dell'Aira, F., & Meier, C. I. (2025). Beyond total impervious area: A new lumped descriptor of basin-wide hydrologic connectivity for characterizing urban watersheds. *Hydrology and Earth System Sciences, 29*(4), 1001-1032. https://doi.org/10.5194/hess-29-1001-2025

DeSousa, S., Bhaskar, A. S., Kelleher, C., & Livneh, B. (2024). Understanding spatiotemporal patterns and drivers of urban flooding using municipal reports. *Hydrological Processes, 38*(12), Article e70028. https://doi.org/10.1002/hyp.70028

Dewan Negeri Selangor. (2022). *Penyata Jawatankuasa Pilihan Mengenai Pihak Berkuasa Tempatan (JP-PBT) bagi Dewan Negeri Selangor berhubung bencana banjir pada bulan Disember 2021 di Negeri Selangor* (Kertas Bil. 7 Tahun 2022). https://dewan.selangor.gov.my/statement/kertas-bil-7-tahun-2022-jp-pbt-bencana-banjir-pada-bulan-disember-2021-di-negeri-selangor/

Du, J., Cheng, L., Zhang, Q., Yang, Y., & Xu, W. (2019). Different flooding behaviors due to varied urbanization levels within river basin: A case study from the Xiang River basin, China. *International Journal of Disaster Risk Science, 10*(1), 89-102. https://doi.org/10.1007/s13753-018-0195-4

Du, S., Shi, P., Van Rompaey, A., & Wen, J. (2015). Quantifying the impact of impervious surface location on flood peak discharge in urban areas. *Natural Hazards, 76*(3), 1457-1471. https://doi.org/10.1007/s11069-014-1463-2

Dwivedi, D., Poeppl, R. E., & Wohl, E. (2025). Hydrological connectivity: A review and emerging strategies for integrating measurement, modeling, and management. *Frontiers in Water, 7*, Article 1496199. https://doi.org/10.3389/frwa.2025.1496199

Feng, B., Wang, J., Zhang, Y., Hall, B., & Zeng, C. (2020). Urban flood hazard mapping using a hydraulic–GIS combined model. *Natural Hazards, 100*(3), 1089-1104. https://doi.org/10.1007/s11069-019-03850-7

Fernández, D. S., & Lutz, M. A. (2010). Urban flood hazard zoning in Tucumán province, Argentina, using GIS and multicriteria decision analysis. *Engineering Geology, 111*(1-4), 90-98. https://doi.org/10.1016/j.enggeo.2009.12.006

Gebremichael, A., Gebremariam, E., & Desta, H. (2025). GIS-based mapping of flood hazard areas and soil erosion using analytic hierarchy process (AHP) and the universal soil loss equation (USLE) in the Awash River basin, Ethiopia. *Geoscience Letters, 12*(1), Article 12. https://doi.org/10.1186/s40562-025-00382-w

Goumghar, L., Fri, R., Hajaj, S., Taia, S., & El Mansouri, B. (2025). Integrating geospatial data and analytic hierarchy process for flood-prone zones mapping in the Upper Draa basin, Morocco. *Ecological Engineering & Environmental Technology, 26*(4), 251-268. https://doi.org/10.12912/27197050/201160

Guo, K., & Guan, M. (2022). Physical complexity to model rainfall-driven urban surface water flooding. In *Proceedings of the 39th IAHR World Congress* (pp. 4667-4671). International Association for Hydro-Environment Engineering and Research. https://doi.org/10.3850/IAHR-39WC252171192022246

Haghizadeh, A., Siahkamari, S., Haghiabi, A. H., & Rahmati, O. (2017). Forecasting flood-prone areas using Shannon's entropy model. *Journal of Earth System Science, 126*(3), Article 39. https://doi.org/10.1007/s12040-017-0819-x

Halim, B. M. K., Shamsuddin, N. S. A., Abdullah, R., & Kamarudin, K. H. (2024). Factors contributing to participation in community-led DRR programmes in Malaysia. *Disaster Advances, 17*(8), 41-48. https://doi.org/10.25303/178da041048

Hassan, B. T., Yassine, M., & Amin, D. (2022). Comparison of urbanization, climate change, and drainage design impacts on urban flashfloods in an arid region: Case study, New Cairo, Egypt. *Water, 14*(15), Article 2430. https://doi.org/10.3390/w14152430

Islam, T., Zeleke, E. B., Afroz, M., & Melesse, A. M. (2025). A systematic review of urban flood susceptibility mapping: Remote sensing, machine learning, and other modeling approaches. *Remote Sensing, 17*(3), Article 524. https://doi.org/10.3390/rs17030524

Khan, A. A., Driss, M., Boulila, W., Sampedro, G. A., Abbas, S., & Wechtaisong, C. (2024). Privacy preserved and decentralized smartphone recommendation system. *IEEE Transactions on Consumer Electronics, 70*(1), 4617-4624. https://doi.org/10.1109/TCE.2023.3323406

Khan, A. A., Faheem, M., Bashir, R. N., Wechtaisong, C., & Abbas, M. Z. (2022). Internet of things (IoT) assisted context aware fertilizer recommendation. *IEEE Access, 10*, 129505-129519. https://doi.org/10.1109/ACCESS.2022.3228160

Khan, A. A., Nauman, M. A., Bashir, R. N., Jahangir, R., Alroobaea, R., Binmahfoudh, A., Alsafyani, M., & Wechtaisong, C. (2022). Context aware evapotranspiration (ETs) for saline soils reclamation. *IEEE Access, 10*, 110050-110063. https://doi.org/10.1109/ACCESS.2022.3206009

Khan, Q., Kalbus, E., Zaki, N., & Mohamed, M. M. (2022). Utilization of social media in floods assessment using data mining techniques. *PLOS ONE, 17*(4), Article e0267079. https://doi.org/10.1371/journal.pone.0267079

Komori, D., Nakaguchi, K., Inomata, R., Oyatsu, Y., Tachikawa, R., & Kazama, S. (2022). Topographical characteristics of frequent urban pluvial flooding areas in Osaka and Nagoya cities, Japan. *Water, 14*(18), Article 2795. https://doi.org/10.3390/w14182795

Lane, S. N., Reaney, S. M., & Heathwaite, A. L. (2009). Representation of landscape hydrological connectivity using a topographically driven surface flow index. *Water Resources Research, 45*(8), Article W08423. https://doi.org/10.1029/2008WR007336

Leopold, L. B., Wolman, M. G., & Miller, J. P. (1964). *Fluvial processes in geomorphology*. W. H. Freeman.

Liu, N., & Zhang, F. (2025). Urban green spaces and flood disaster management: Toward sustainable urban design. *Frontiers in Public Health, 13*, Article 1583978. https://doi.org/10.3389/fpubh.2025.1583978

Liu, R., Chen, Y., Wu, J., Gao, L., Barrett, D., Xu, T., Li, X., Li, L., Huang, C., & Yu, J. (2017). Integrating entropy-based naïve Bayes and GIS for spatial evaluation of flood hazard. *Risk Analysis, 37*(4), 756-773. https://doi.org/10.1111/risa.12698

Malekinezhad, H., Sepehri, M., Pham, Q. B., Hosseini, S. Z., Meshram, S. G., Vojtek, M., & Vojteková, J. (2021). Application of entropy weighting method for urban flood hazard mapping. *Acta Geophysica, 69*(3), 841-854. https://doi.org/10.1007/s11600-021-00586-6

Manandhar, B., Cui, S., Wang, L., & Shrestha, S. (2023). Urban flood hazard assessment and management practices in South Asia: A review. *Land, 12*(3), Article 627. https://doi.org/10.3390/land12030627

Moore, I. D., Grayson, R. B., & Ladson, A. R. (1991). Digital terrain modelling: A review of hydrological, geomorphological, and biological applications. *Hydrological Processes, 5*(1), 3-30. https://doi.org/10.1002/hyp.3360050103

Muhamad Azizi, M. A. A., & Teriman, S. (2023). The consequences and mitigation of floods affecting Taman Sri Muda, Shah Alam. In *e-Proceeding of 6th Undergraduate Seminar on Built Environment and Technology (USBET) 2023* (pp. 1931-1940). Universiti Teknologi MARA. https://ir.uitm.edu.my/id/eprint/95286/

Nizar, N., Hariyani, S., Rahmasari, P., Rafani, M., Hidayati, E., & Arianti, I. (2024). Integration of digital elevation model (DEM) for accurate slope and contour maps as fundamental data in spatial modeling. *International Journal of Research Publication and Reviews, 5*(3), 7011-7015. https://doi.org/10.55248/gengpi.5.0324.0890

Nooryati. (2022, October 18). *Bencana banjir kilat di Selangor, faktor perubahan iklim?* Institut Pengajian Sains Sosial, Universiti Putra Malaysia. https://ipsas.upm.edu.my/artikel/bencana_banjir_kilat_di_selangor_faktor_perubahan_iklim-69663

Ogden, F. L., Pradhan, N. R., Downer, C. W., & Zahner, J. A. (2011). Relative importance of impervious area, drainage density, width function, and subsurface storm drainage on flood runoff from an urbanized catchment. *Water Resources Research, 47*(12), Article W12503. https://doi.org/10.1029/2011WR010550

Pimenta, L., Duarte, L., Teodoro, A. C., Beltrão, N., Gomes, D., & Oliveira, R. (2025). GIS-based flood susceptibility mapping using AHP in the urban Amazon: A case study of Ananindeua, Brazil. *Land, 14*(8), Article 1543. https://doi.org/10.3390/land14081543

Rosmadi, H. S., Ahmed, M. F., Mokhtar, M. B., & Lim, C. K. (2023). Reviewing challenges of flood risk management in Malaysia. *Water, 15*(13), Article 2390. https://doi.org/10.3390/w15132390

Sepehri, M., Malekinezhad, H., Hosseini, S. Z., & Ildoromi, A. R. (2019). Assessment of flood hazard mapping in urban areas using entropy weighting method: A case study in Hamadan city, Iran. *Acta Geophysica, 67*(5), 1435-1449. https://doi.org/10.1007/s11600-019-00342-x

Sharma, A., Poonia, M., Rai, A., Biniwale, R. B., Tügel, F., Holzbecher, E., & Hinkelmann, R. (2024). Flood susceptibility mapping using GIS-based frequency ratio and Shannon's entropy index bivariate statistical models: A case study of Chandrapur district, India. *ISPRS International Journal of Geo-Information, 13*(8), Article 297. https://doi.org/10.3390/ijgi13080297

Singh, P., Sinha, V. S. P., Vijhani, A., & Pahuja, N. (2018). Vulnerability assessment of urban road network from urban flood. *International Journal of Disaster Risk Reduction, 28*, 237-250. https://doi.org/10.1016/j.ijdrr.2018.03.017

Singh, V. P. (1997). The use of entropy in hydrology and water resources. *Hydrological Processes, 11*(6), 587–626. https://doi.org/10.1002/(SICI)1099-1085(199705)11:6%3C587::AID-HYP479%3E3.0.CO;2-P

Tang, Z., Zhang, H., Yi, S., & Xiao, Y. (2018). Assessment of flood susceptible areas using spatially explicit, probabilistic multi-criteria decision analysis. *Journal of Hydrology, 558*, 144-158. https://doi.org/10.1016/j.jhydrol.2018.01.033

Ullah, F., Pun, C.-M., Mohmand, M. I., Mahendran, R. K., Khan, A. A., Alhammad, S. M., Rodrigues, J. J. P. C., & Farouk, A. (2025). Privacy-aware secure data auditing for cloud-based intelligence of things environment. *IEEE Internet of Things Journal, 12*(11), 15288-15303. https://doi.org/10.1109/JIOT.2025.3528117

Wehn, U., Rusca, M., Evers, J., & Lanfranchi, V. (2015). Participation in flood risk management and the potential of citizen observatories: A governance analysis. *Environmental Science & Policy, 48*, 225-236. https://doi.org/10.1016/j.envsci.2014.12.017

Yusuf, A., Ojo, R., Idrees, M. O., Balogun, A.-L., Salami, I. B., & Sani, O. S. (2023). Modelling flood hazards impacted by ungauged river in urbanised area using HEC-RAS and GIS. *Nigerian Journal of Technological Development, 20*(2), 83-92. https://doi.org/10.4314/njtd.v20i2.1405

Zhou, Q. (2014). A review of sustainable urban drainage systems considering the climate change and urbanization impacts. *Water, 6*(4), 976-992. https://doi.org/10.3390/w6040976

Zhou, R., Zheng, H., Liu, Y., Xie, G., & Wan, W. (2022). Flood impacts on urban road connectivity in southern China. *Scientific Reports, 12*(1), Article 16866. https://doi.org/10.1038/s41598-022-20882-5